

PAPER • OPEN ACCESS

# Graphene-diamond junction photoemission microscopy and electronic interactions

To cite this article: Gary Wan *et al* 2020 *Nano Express* **1** 020011

View the [article online](#) for updates and enhancements.



## PAPER

## Graphene-diamond junction photoemission microscopy and electronic interactions

## OPEN ACCESS

RECEIVED  
6 June 2020REVISED  
3 July 2020ACCEPTED FOR PUBLICATION  
9 July 2020PUBLISHED  
23 July 2020

Original content from this work may be used under the terms of the [Creative Commons Attribution 4.0 licence](#).

Any further distribution of this work must maintain attribution to the author(s) and the title of the work, journal citation and DOI.

Gary Wan<sup>1,2</sup> , Sanjeevani Panditharatne<sup>2</sup>, Neil A Fox<sup>1,2,3</sup> and Mattia Cattelan<sup>3</sup> <sup>1</sup> Bristol Centre for Functional Nanomaterials, University of Bristol, Tyndall Avenue, Bristol, BS8 1TL, United Kingdom<sup>2</sup> School of Physics, HH Wills Physics Laboratory, University of Bristol, Tyndall Avenue, Bristol, BS8 1TL, United Kingdom<sup>3</sup> School of Chemistry, University of Bristol, Cantocks Close, Bristol, BS8 1TS, United KingdomE-mail: [mattia.cattelan@bristol.ac.uk](mailto:mattia.cattelan@bristol.ac.uk)

Keywords: graphene, diamond, ARPES, PEEM, Schottky barrier

**Abstract**

Polycrystalline graphene was transferred onto differently terminated epitaxial layers of boron-doped diamond deposited onto single crystal substrates. Chemical and electronic characterisation was performed using energy-filtered photoemission electron microscopy and angle-resolved photoemission spectroscopy. Electronic interaction between the diamond and graphene was observed, where doping of the graphene on the hydrogen and oxygen terminated diamond was n-doping of 250 meV and 0 meV respectively. We found that the wide window of achievable graphene doping is effectively determined by the diamond surface dipole, easily tuneable with a varying surface functionalisation. A Schottky junction using the graphene-diamond structure was clearly observed and shown to reduce downward band bending of the hydrogen terminated diamond, producing a Schottky barrier height of 330 meV.

**1. Introduction**

Graphene is known for its superior performance in electronic applications over traditional materials, such as its thermal conductivity [1], strength [2], electronic mobility [3] and thermal stability [4]. While these properties have been well studied and understood, the implementation of graphene electronics has faced certain challenges, in particular the lack of a band gap and low density of states at its intrinsic Fermi level [5, 6]. These lead to difficulty in current controllability in conventional field-effect transistors and reduced intrinsic conductivity. Some techniques have been developed towards overcoming these difficulties, such as band gap engineering [7] and doping [8], however they have been shown to be difficult; often hindering the intrinsic electronic transport properties of graphene.

The interactions of other materials with graphene have applications from catalysis [9] to plasmonics [10, 11], utilising graphene's excellent electron acceptor and transport properties. These are achievable due to graphene's readiness to form van der Waals interactions [12, 13], and its well understood two-dimensional band structure allowing easier manipulation. Here we investigate the electronic properties of a heterojunction of graphene on diamond, a wide band gap semiconductor, which potentially provides an alternative solution to some of the challenges mentioned above. Graphene on diamond has already shown to improve its current carrying capability [14, 15], and in some cases purely from the enhanced thermal conductivity [16] without involving any electronic modifications. In this study we focus on the electronic changes in both the underlying single crystal diamond substrate and the graphene layer, their tuneability with simple alterations to the diamond surface functionalisation and prediction of further changes with the use of different substrates.

Charge transfer across an interface plays a major role in the electronic changes of a material, leading to effects such as doping or band bending. This is an active area of research for diamond where adsorbates are introduced to the surface for surface transfer doping, inducing a surface p-type conductivity [17]. It is possible in part due to diamond's wide bandgap and ability to exhibit either a negative (NEA) or positive electron affinity (PEA) [18], which can also prove advantageous as a tuneable substrate for graphene doping. A graphene-diamond interface

will also act as a Schottky barrier junction, allowing for potential use as a rectifying device or transistor [13]. While a gate-controlled graphene-silicon Schottky barrier structure has been shown to exhibit promising logic operation behaviour [19].

We explore the effects of a graphene-diamond junction by transferring single-layer polycrystalline graphene onto single crystal diamond substrates, with electrical measurements acquired using advanced photoemission spectroscopy. The diamond substrates were boron doped for electrical conductivity and terminated with either hydrogen or oxygen.

## 2. Experimental

### 2.1. Diamond preparation

Single-crystal diamond (111) substrates were purchased from Euro Superabrasives (MM 111/4010). Boron-doped layers were grown onto each substrate using an Applied Science and Technology (ASTeX)-type microwave plasma-enhanced chemical vapor deposition (CVD) reactor for 10 min, using 3% CH<sub>4</sub> and 3 ppm B<sub>2</sub>H<sub>6</sub> in H<sub>2</sub> to produce a conductive film, at 1300 W and 130 Torr between 960 and 990 °C.

Hydrogen-termination was performed in the growth reactor with a pure hydrogen plasma at 900 °C for 2 min, followed by 2 min at 500 °C. Oxygen-termination was done via a 30 min ultraviolet-ozone treatment.

After the deposition, the diamond films were characterised using photoemission electron microscopy (PEEM) and angle-resolved photoemission spectroscopy (ARPES) to prove they had a satisfactory level of epitaxial growth. Details of the grown films are contained within a previous paper using identical growth conditions [18].

### 2.2. Graphene transfer

The polycrystalline graphene on Cu foil was purchased from Graphene Laboratories Inc., synthesized by methane decomposition [20–22]. Two distinctive main azimuthal orientations of graphene flakes, about 60° apart, were observed here in full-wavevector ARPES acquisitions. Due to this measurement, we can infer that the copper foil mainly constituted Cu (111) grains and graphene was grown at relatively low temperatures (900 °C) [23]. We cannot exclude the presence of small multilayers with several different azimuthal orientations [24, 25].

The polycrystalline graphene layer on Cu was transferred onto single crystal diamond substrates following the well-known wet transfer method which can be found with different variations [23, 26–28]. In this work we followed the methods of Liang *et al* [29] where the graphene/copper sample was spin coated with PMMA to perform a PMMA-mediated transfer using an etching solution of 0.2 M Fe(NO<sub>3</sub>)<sub>3</sub>(aq). Samples were cleaned using a modified RCA method requiring submersion in standard solutions of 20:1:1 H<sub>2</sub>O:H<sub>2</sub>O<sub>2</sub>:HCl for 15 min at room temperature (RT) followed by 20:1:1 H<sub>2</sub>O:H<sub>2</sub>O<sub>2</sub>:NH<sub>4</sub>OH for 15 min at RT before being thoroughly rinsed in deionised water. The graphene/PMMA stack was picked up by the target substrate while immersed in a bath of distilled water and then baked for 15 min at 150 °C. The PMMA scaffold was removed through immersion in an acetone bath for 1 h, before being rinsed with isopropyl and dried with N<sub>2</sub>. The sample was then baked again at 200 °C for 10 min.

### 2.3. Surface analysis

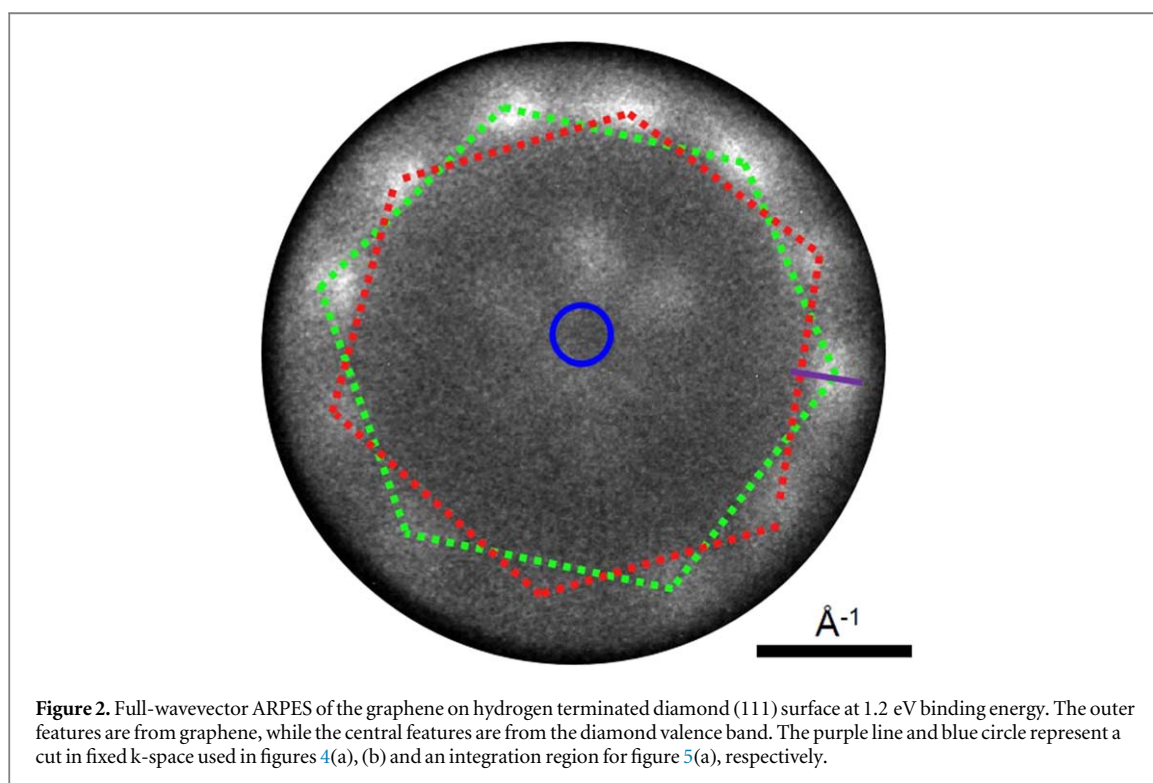
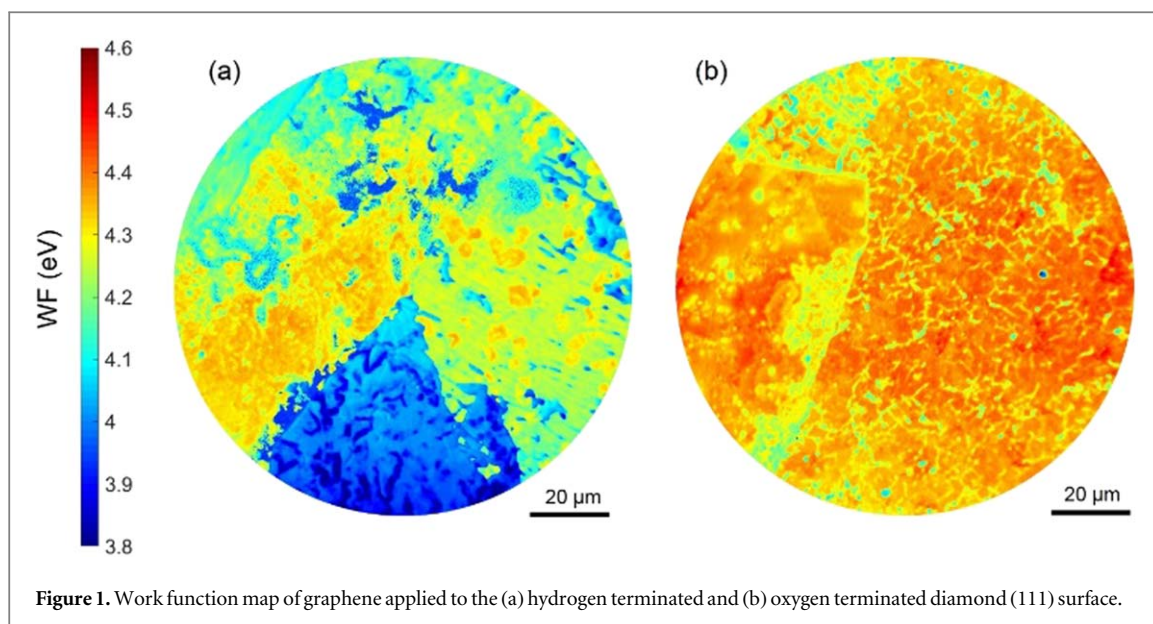
The prepared samples were then transferred into the Bristol NanoESCA Facility's ultra-high vacuum (UHV) chambers, where they were annealed at 450 °C overnight and remained under UHV conditions for the duration of the experiment.

A NanoESCA II energy-filtered PEEM (EF-PEEM) was used for full-wavevector ARPES and work function (WF) mapping, all the measurements were acquired at RT. A non-monochromatic Hg source ( $h\nu \approx 5.2$  eV) was used for the WF mapping, while a monochromated He-I ( $h\nu = 21.2$  eV) vacuum ultraviolet (VUV) light source was used for ARPES and dark-field photoemission electron microscopy (DF-PEEM). The overall energy resolution is about 120 meV; the lateral resolution for the WF maps were better than 150 nm, while DF imaging of diamond and graphene showed details of about 600 nm and 1.9 μm respectively.

The samples are mounted and electrically connected to the sample holders with a Mo washer pressed down on the sample surface. During measurements, the sample is biased relative to the analyser for energy-filtering, which was previously calibrated using a single-crystal copper sample.

## 3. Results and discussion

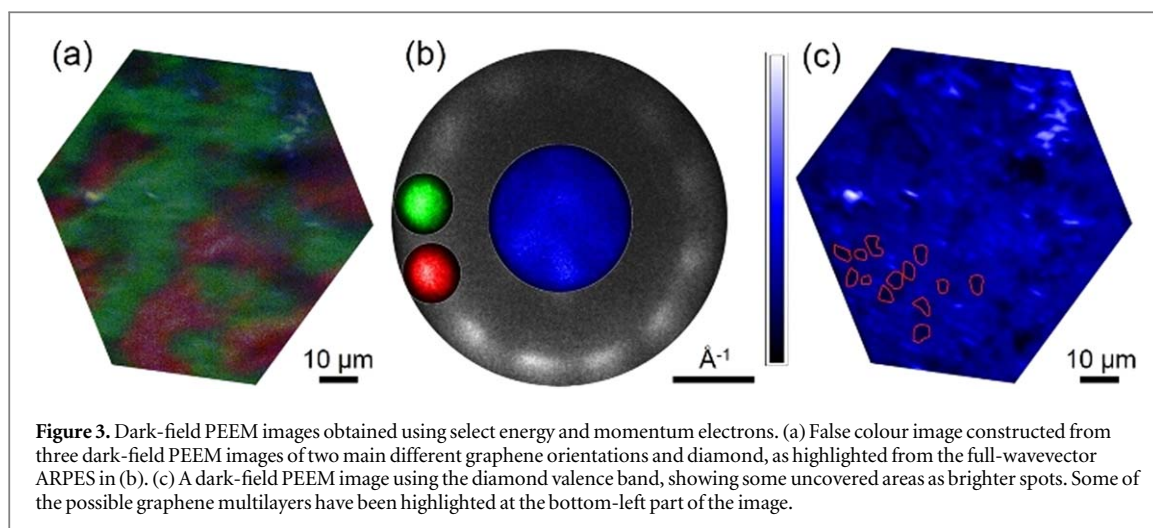
We begin our investigation with WF analysis of the graphene-diamond surfaces to better understand the achieved microscopic structure, figure 1. This is important as the graphene coverage and the WF changes can be crucial in the further analysis of the electronic structure of the junction. WF maps of the samples were generated from fitting EF-PEEM images close to the WF cut-off edge, using a pixel-by-pixel gradient extrapolation to the



background. The WF values were then corrected for the Schottky effect of 98 meV due to the high PEEM extractor field of 12 kV over a 1.8 mm sample distance [30]. The bottom sector of the WF map of the hydrogen terminated diamond surface in figure 1(a) has a noticeably lower WF than the diamond covered by graphene. This stark contrast in WF, between the covered and uncovered diamond surface, is one simple method for identifying graphene coverage. Figure 1(b) shows a more uniform graphene coverage, with a separation visible between the two adjoining macro-areas discussed later.

Figure 2 shows a full-wavevector ARPES of graphene on a hydrogen terminated diamond (111) substrate at 1.2 eV binding energy.

This acquisition reveals two main azimuthal orientations at about  $60^\circ$  of the transferred polycrystalline graphene as grown on copper [23] (see Materials and Methods). As stated above we cannot exclude the presence of small regions with multilayers of different orientations, which can cause elongated Dirac cones and a reduction in sharpness of the graphene features. Features seen in the centre are from the diamond bulk band structure, while the twelve outer circles are from the Dirac cones of two main graphene orientations (green and



red dotted lines). While clearly distinguishable in ARPES, the WF maps from the corresponding real-space field-of-view do not show a visible distinction between the two graphene orientations, as shown in figure 1. Selective imaging can be achieved by using specific electron energy and momentum for imaging the band structure [31]. Figure 3(b) shows the regions used in the full-wavevector ARPES to separately image the diamond and graphene orientations, on the graphene covered hydrogen terminated diamond (111) substrate. Figure 3(a) is the combination of a diamond and two graphene DF-PEEM images. The green and red areas cover most of the entire surface, as expected for graphene on copper, and show a similar coverage of both orientations without great overlap. Graphene grains with similar orientations have dimensions ranging from about 2 to 30  $\mu\text{m}$  indicating that the much larger macro-areas observed on the WF maps (figure 1(b)) are likely due to the copper foil grains they were grown on. The diamond DF-PEEM image (figure 3(c)) confirms that electrons originating from the diamond surface can still pass through the overlaying graphene, although an increase in signal is observed for areas without graphene. Considering the extreme surface sensitivity of ARPES with VUV excitation [32], the visible diamond structure also ensures a direct contact between the analysed graphene and diamond surface, without noticeable contamination at the interface.

The darker patches circled in figure 3(c) could indicate the presence of small multilayers roughly 5  $\mu\text{m}$  wide; indeed, thicker multiple graphene layers are expected to attenuate the diamond signal more than a single layer. However, no increase in the graphene signal is seen in the potential multilayer areas. This is to be expected due to the azimuthally disoriented nature of multilayer graphene on copper [25], whereas the red and green images in figure 3(a) are acquired from selecting only precise orientations. Brighter areas of figure 3(a) can be considered macro-defects of the substrate which pierced the transferred graphene layers. Shape and dimension of these areas are similar to the low-WF spots visible near the top of figure 1(a).

After studying the sample morphology, we continue our investigation on the heterojunction electrical effects. A cut in k-space along the purple line in figure 2 shows the energy dispersive band structure of the graphene-diamond structure, shown in figure 4(a). The Dirac point is situated at 250 meV binding energy, indicating an n-type doping of the graphene. This is due to surface transfer of electrons from the diamond surface to the graphene [33], driven by the difference in their electrochemical potential. This has also been reported for graphene on phosphorus doped diamond [34].

Hydrogen termination of diamond induces a downward band bending and WF reduction, due to surface dipole formation [18, 35], allowing the diamond to act as an electron donor for the graphene. The low density of states at the graphene Fermi level and large WF difference between the hydrogen terminated diamond and graphene contribute to the large doping of the graphene. This is exemplified by using an oxygen terminated diamond substrate, shown in figure 4(b), where no noticeable doping is observed. This change in doping is expected due to the increased diamond WF from the replacement of hydrogen termination with oxygen [36]. The graphene WF on oxygen terminated diamond was found to be around 4.4–4.5 eV, similar to its intrinsic value [37, 38]. The difference in doping between using the two different substrates is also clearly visible when performing a line profile at the graphene K point (figure 4(c)).

Cutting along a different set of Dirac cones than the one reported in figure 2, i.e. a different azimuthal orientation of graphene, shows no clear difference in doping within our energy resolution. Moreover, similar analysis of graphene on hydrogen terminated diamond (100) results to similar doping and WF. These findings

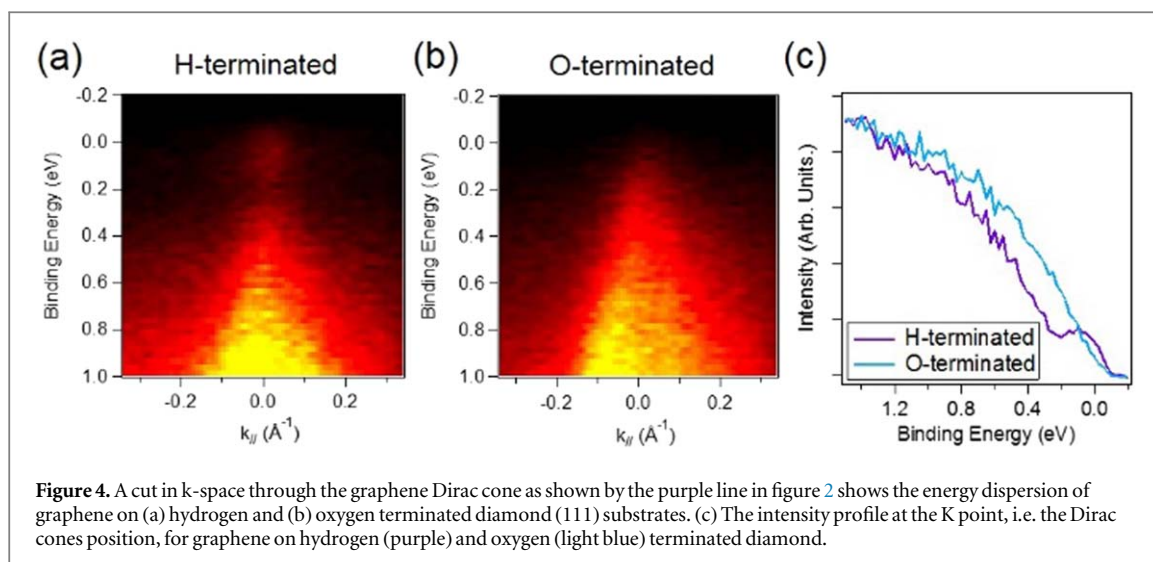


**Figure 4.** A cut in  $k$ -space through the graphene Dirac cone as shown by the purple line in figure 2 shows the energy dispersion of graphene on (a) hydrogen and (b) oxygen terminated diamond (111) substrates. (c) The intensity profile at the K point, i.e. the Dirac cones position, for graphene on hydrogen (purple) and oxygen (light blue) terminated diamond.

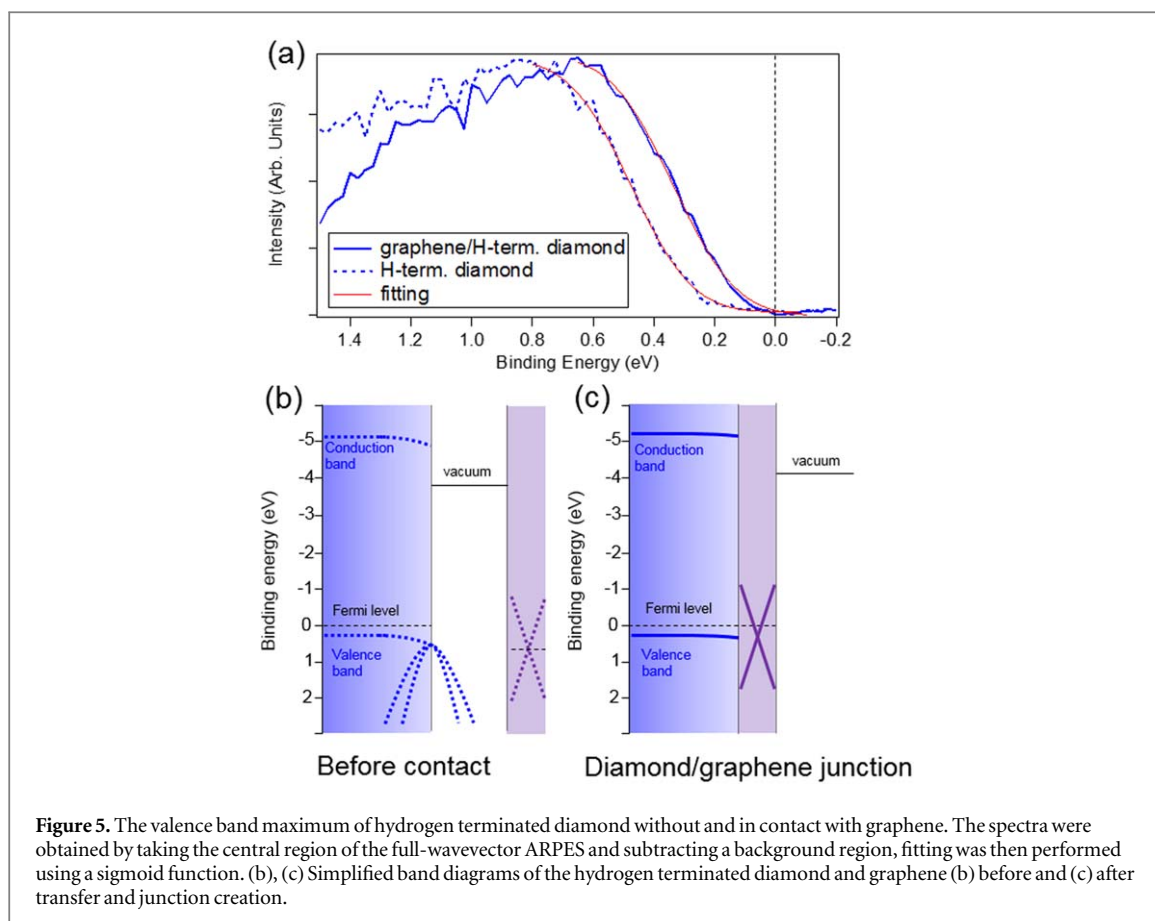
indicate that the interaction with graphene and diamond is independent of the materials' respective orientations. Furthermore, within our experimental resolution we did not observe any interaction between the graphene and diamond band structures when the two overlap at about 3–4 eV in binding energy. While this could be caused by the weak signal from the diamond, a lack of state hybridisation could suggest no out-of-plane orbital characteristics in diamond bands, preventing them from interacting effectively with the graphene  $\pi$  bands [39]. This finding likely indicates that the interactions examined are dominated by electrostatic interaction.

The WF difference of graphene on the hydrogen and oxygen terminated substrates in figure 1 is approximately 200 meV; similar to the doping difference between the two graphene layers. This suggests a purely electronic effect mediated by charge transfer across the interface that is dependent on the WF difference, density of states and overall geometry of the system [25, 37]. We believe a window of graphene doping is thus achievable by simply using partial hydrogen and oxygen diamond terminations [18].

As graphene acts as a metal, and diamond a semiconductor, the graphene-diamond interface can also act as a Schottky junction. Band bending occurs naturally at diamond surfaces due to the existence of surface states, often leading to Fermi-level pinning [40, 41]. The application of graphene onto the diamond surfaces alters the occupancy of the diamond surface states, and thus the surface band bending. The Schottky barrier height, i.e. the energy difference between the metal (graphene) Fermi level (0 eV binding energy) and the edge of the semiconductor (diamond) majority carrier band (valence band) [13], can be obtained through precise determination of the diamond valence band maximum position from the ARPES spectra [42]. A small region of interest containing the diamond valence band maximum at the  $\Gamma$  point, i.e. the blue circle in the full-wavevector ARPES in figure 2, can be subtracted by a background region between the diamond and graphene structures, providing a spectrum for determining the valence band maximum position (figure 5(a)). Compared with the bare hydrogen terminated diamond substrate, the graphene induces a notable amount of band bending on the diamond surface, reducing the binding energy of the valence band maximum by about 150 meV. The band diagram in figures 5(b), (c) depicts the graphene and hydrogen terminated diamond (b) before and (c) after the transfer. A downward surface band bending exists on the diamond initially due to the boron doping and surface termination [41], while the Fermi level is above that of the graphene. This drives the electron transfer across the junction, which in turn reduces the diamond downward band bending as well as dope the graphene. The Schottky barrier height is determined to be 330 meV for graphene on a hydrogen terminated boron doped diamond (111) substrate.

## 4. Conclusions

Tunable electronic doping of graphene can be achieved within a 250 meV window using surface functionalised diamond substrates. Oxygen and hydrogen terminated boron doped diamond act as a platform to modulate the graphene properties, using the previously demonstrated surface dipole and electronic property tunability of this type of material [18]. Boron doped diamond was used in this paper to provide the necessary conductivity for photoemission experiments; however, we expect that nitrogen or phosphorus doping can further reduce the diamond WF and increase the graphene n-type doping [34, 43, 44]. A p-type doping and greater Schottky barrier



height can also be expected from greater electron affinity diamond surface terminations, such as fluorine [40, 45]. An atomically flat and clean diamond-graphene interface with a bare diamond termination may also demonstrate unique properties, achievable with vacuum annealing of diamond (111) substrates [46]. The Schottky barrier height has been calculated for hydrogen terminated diamond demonstrating that our measurements can clearly visualise the effect of the heterojunction in both materials.

## Acknowledgments

The authors acknowledge Bristol NanoESCA Facility (EPSRC Strategic Equipment Grant EP/K035746/1 and EP/M000605/1) where experiments were carried out. G.W. acknowledges the PhD studentship funded through BCFN: Renewtec Technologies, Al Hamad Group.

## ORCID iDs

Gary Wan <https://orcid.org/0000-0003-3423-1440>

Mattia Cattelan <https://orcid.org/0000-0001-9314-1475>

## References

- [1] Balandin A A, Ghosh S, Bao W, Calizo I, Teweldebrhan D, Miao F and Lau C N 2008 Superior thermal conductivity of single-layer graphene *Nano Lett.* **8** 902–7
- [2] Lee C, Wei X, Kysar J W and Hone J 2008 Measurement of the elastic properties and intrinsic strength of monolayer graphene *Science (80-.)* **321** 385–8
- [3] Novoselov K S 2004 Electric field effect in atomically thin carbon films *Science (80-.)* **306** 666–9
- [4] Los J H, Zakharchenko K V, Katsnelson M I and Fasolino A 2015 Melting temperature of graphene *Phys. Rev. B* **91** 045415
- [5] Schwierz F 2013 Graphene transistors: status, prospects, and problems *Proc. IEEE* **101** 1567–84
- [6] Liu H, Liu Y and Zhu D 2011 Chemical doping of graphene *J. Mater. Chem.* **21** 3335–45
- [7] Han M Y, Özyilmaz B, Zhang Y and Kim P 2007 Energy band-gap engineering of graphene nanoribbons *Phys. Rev. Lett.* **98** 206805
- [8] Wei D, Liu Y, Wang Y, Zhang H, Huang L and Yu G 2009 Synthesis of N-doped graphene by chemical vapor deposition and its electrical properties *Nano Lett.* **9** 1752–8

- [9] Xiang Q, Yu J and Jaroniec M 2012 Graphene-based semiconductor photocatalysts *Chem. Soc. Rev.* **41** 782–96
- [10] Grigorenko A N, Polini M and Novoselov K S 2012 Graphene plasmonics *Nat. Photonics* **6** 749–58
- [11] Yan H, Li X, Chandra B, Tulevski G, Wu Y, Freitag M, Zhu W, Avouris P and Xia F 2012 Tunable infrared plasmonic devices using graphene/insulator stacks *Nat. Nanotechnol.* **7** 330–4
- [12] Liu Y, Guo J, Zhu E, Liao L, Lee S-J, Ding M, Shakir I, Gambin V, Huang Y and Duan X 2018 Approaching the Schottky–Mott limit in van der Waals metal–semiconductor junctions *Nature* **557** 696–700
- [13] Di Bartolomeo A 2016 Graphene Schottky diodes: an experimental review of the rectifying graphene/semiconductor heterojunction *Phys. Rep.* **606** 1–58
- [14] Zhao F, Thuong Nguyen T, Golsharifi M, Amakubo S, Loh K P and Jackman R B 2013 Electronic properties of graphene-single crystal diamond heterostructures *J. Appl. Phys.* **116** 109901
- [15] Hu W, Li Z and Yang J 2013 Diamond as an inert substrate of graphene *J. Chem. Phys.* **138** 054701
- [16] Yu J, Liu G, Sumant A V, Goyal V and Balandin A A 2012 Graphene-on-diamond devices with increased current-carrying capacity: carbon sp<sup>2</sup>-on-sp<sup>3</sup> technology *Nano Lett.* **12** 1603–8
- [17] Edmonds M T, Pakes C I, Mammadov S, Zhang W, Tadich A, Ristein J and Ley L 2011 Work function, band bending, and electron affinity in surface conducting (100) diamond *Phys. Status Solidi* **208** 2062–6
- [18] Wan G, Cattelan M and Fox N A 2019 Electronic structure tunability of diamonds by surface functionalization *J. Phys. Chem. C* **123** 4168–77
- [19] Yang H, Heo J, Park S, Song H J, Seo D H, Byun K-E, Kim P, Yoo I, Chung H-J and Kim K 2012 Graphene barristor, a triode device with a gate-controlled schottky barrier *Science (80-.)* **336** 1140–3
- [20] Losurdo M, Giangregorio M M, Capezzuto P and Bruno G 2011 Graphene CVD growth on copper and nickel: role of hydrogen in kinetics and structure *Phys. Chem. Chem. Phys.* **13** 20836
- [21] Cattelan M, Agnoli S, Favaro M, Garoli D, Romanato F, Meneghetti M, Barinov A, Dudin P and Granozzi G 2013 Microscopic view on a chemical vapor deposition route to boron-doped graphene nanostructures *Chem. Mater.* **25** 1490–5
- [22] Mattevi C, Kim H and Chhowalla M 2011 A review of chemical vapour deposition of graphene on copper *J. Mater. Chem.* **21** 3324–34
- [23] Hu B, Ago H, Ito Y, Kawahara K, Tsuji M, Magome E, Sumitani K, Mizuta N, Ikeda K and Mizuno S 2012 Epitaxial growth of large-area single-layer graphene over Cu(111)/sapphire by atmospheric pressure CVD *Carbon N. Y.* **50** 57–65
- [24] Zhou L et al 2018 Surface structure of few layer graphene *Carbon N. Y.* **136** 255–61
- [25] Peng H et al 2017 Substrate doping effect and unusually large angle van Hove singularity evolution in twisted Bi- and multilayer graphene *Adv. Mater.* **29** 1606741
- [26] He Y et al 2014 Metal-film-assisted ultra-clean transfer of single-walled carbon nanotubes *Nano Res.* **7** 981–9
- [27] Jiao L, Fan B, Xian X, Wu Z, Zhang J and Liu Z 2008 Creation of nanostructures with poly(methyl methacrylate)-mediated nanotransfer printing *J. Am. Chem. Soc.* **130** 12612–3
- [28] An C J, Kim S J, Choi H O, Kim D W, Jang S W, Jin M L, Park J-M, Choi J K and Jung H-T 2014 Ultraclean transfer of CVD-grown graphene and its application to flexible organic photovoltaic cells *J. Mater. Chem. A* **2** 20474–80
- [29] Liang X et al 2011 Toward clean and crackless transfer of graphene *ACS Nano* **5** 9144–53
- [30] Mathieu C, Barrett N, Rault J, Mi Y Y, Zhang B, de Heer W A, Berger C, Conrad E H and Renault O 2011 Microscopic correlation between chemical and electronic states in epitaxial graphene on SiC(000 $\bar{1}$ ) *Phys. Rev. B* **83** 235436
- [31] Barrett N, Conrad E, Winkler K and Krömker B 2012 Dark field photoelectron emission microscopy of micron scale few layer graphene *Rev. Sci. Instrum.* **83** 083706
- [32] Lv B, Qian T and Ding H 2019 Angle-resolved photoemission spectroscopy and its application to topological materials *Nat. Rev. Phys.* **1** 609–26
- [33] Chen W, Chen S, Qi D C, Gao X Y and Wee A T S 2007 Surface transfer p-type doping of epitaxial graphene *J. Am. Chem. Soc.* **129** 10418–22
- [34] Yamada T, Masuzawa T, Mimura H and Okano K 2019 Field emission spectroscopy measurements of graphene/n-type diamond heterojunction *Appl. Phys. Lett.* **114** 231601
- [35] Bandis C and Pate B B 1995 Photoelectric emission from negative-electron-affinity diamond (111) surfaces: exciton breakup versus conduction-band emission *Phys. Rev. B* **52** 12056–71
- [36] Loh K P, Xie X N, Yang S W and Zheng J C 2002 Oxygen adsorption on (111)-oriented diamond: a study with ultraviolet photoelectron spectroscopy, temperature-programmed desorption, and periodic density functional theory *J. Phys. Chem. B* **106** 5230–40
- [37] Giovannetti G, Khomyakov P A, Brocks G, Karpan V M, van den Brink J and Kelly P J 2008 Doping graphene with metal contacts *Phys. Rev. Lett.* **101** 026803
- [38] Cattelan M, Vagin M Y, Fox N A, Ivanov I G, Shtepliuk I and Yakimova R 2019 Anodization study of epitaxial graphene: insights on the oxygen evolution reaction of graphitic materials *Nanotechnology* **30** 285701
- [39] Coy Diaz H, Avila J, Chen C, Addou R, Asensio M C and Batzill M 2015 Direct observation of interlayer hybridization and dirac relativistic carriers in graphene/MoS<sub>2</sub> van der Waals heterostructures *Nano Lett.* **15** 1135–40
- [40] Li F, Zhang J, Wang X, Liu Z, Wang W, Li S and Wang H-X 2016 X-ray photoelectron spectroscopy study of Schottky junctions based on oxygen-/fluorine-terminated (100) diamond *Diam. Relat. Mater.* **63** 180–5
- [41] Diederich L, Küttel O M, Aebi P and Schlapbach L 1998 Electron affinity and work function of differently oriented and doped diamond surfaces determined by photoelectron spectroscopy *Surf. Sci.* **418** 219–39
- [42] Baumann P K and Nemanich R J 1998 Electron affinity and Schottky barrier height of metal–diamond (100), (111), and (110) interfaces *J. Appl. Phys.* **83** 2072–82
- [43] Croot A, Wan G, Rowan A, Andrade H D, Smith J A and Fox N A 2017 Beta radiation enhanced thermionic emission from diamond thin films *Front. Mech. Eng.* **3** 1–8
- [44] Sherehiy A, Dumpala S, Sunkara M K, Jasinski J B, Cohn R W and Sumanasekera G U 2014 Thermionic emission from phosphorus (P) doped diamond nanocrystals supported by conical carbon nanotubes and ultraviolet photoelectron spectroscopy study of P-doped diamond films *Diam. Relat. Mater.* **50** 66–76
- [45] Rietwyk K J, Wong S L, Cao L, O'Donnell K M, Ley L, Wee A T S and Pakes C I 2013 Work function and electron affinity of the fluorine-terminated (100) diamond surface *Appl. Phys. Lett.* **102** 091604
- [46] Ogawa S, Yamada T, Ishizuka S, Yoshigoe A, Hasegawa M, Teraoka Y and Takakuwa Y 2012 Vacuum annealing formation of graphene on diamond C(111) surfaces studied by real-time photoelectron spectroscopy *Jpn. J. Appl. Phys.* **51** 11PF02